Gaussianity revisited: exploring the Kibble–Zurek mechanism with superconducting rings

2013 J. Phys.: Condens. Matter 25 404207

(http://iopscience.iop.org/0953-8984/25/40/404207)

J. Phys.: Condens. Matter **25** (2013) 404207 (11pp) doi:10.1088/0953-8984/25/40/404207

Gaussianity revisited: exploring the Kibble–Zurek mechanism with superconducting rings

D J Weir[1], R Monaco[2,3], V P Koshelets[4], J Mygind[5] and R J Rivers[6]

[1] Helsinki Institute of Physics, Gustaf Hällströmin katu 2a, FI-00014 Helsinki, Finland
[2] Istituto di Cibernetica del CNR, Comprensorio Olivetti, I-80078 Pozzuoli, Italy
[3] Facoltà di Scienze, Universitá di Salerno, I-84084 Fisciano, Italy
[4] Kotel'nikov Institute of Radio Engineering and Electronics, Russian Academy of Science, Mokhovaya 11, Bldg 7, 125009 Moscow, Russia
[5] Department of Physics, B309, Technical University of Denmark, DK-2800 Lyngby, Denmark
[6] Blackett Laboratory, Imperial College London, London SW7 2AZ, UK

E-mail: david.weir@helsinki.fi

Received 12 February 2013, in final form 29 April 2013
Published 11 September 2013
Online at stacks.iop.org/JPhysCM/25/404207

Abstract
In this paper we use spontaneous flux production in annular superconductors to shed light on the Kibble–Zurek (KZ) scenario. In particular, we examine the effects of finite size and external fields, neither of which is directly amenable to the KZ analysis. Supported by 1D and 3D simulations, the properties of a superconducting ring are seen to be well represented by analytic Gaussian approximations which encode the KZ scales indirectly. Experimental results for annuli in the presence of external fields corroborate these findings.

(Some figures may appear in colour only in the online journal)

1. Introduction

Causality imposes constraints on systems that are strongly out of equilibrium by restricting the rate of change of correlation lengths to the relevant causal speed (such as the speed of sound). The suggestion that causality would constrain correlation lengths was originally made by Kibble in the context of the very early Universe [1, 2], and by Zurek for condensed matter systems [3, 4]. Frustration is relieved by the spontaneous creation of topological defects, whose separation reflects the correlation lengths at the time of their appearance; this is known as the Kibble–Zurek (KZ) scenario.

This paper focuses on the behaviour of superconducting annuli. An idealization of our experimental setup—which we shall discuss later—is shown in figure 1. To model the system we assume a simple complex scalar field $\phi(x)$ that can act as a proxy for a Cooper pair, decomposed as

$$\phi(x) = |\phi(x)|\mathrm{e}^{\mathrm{i}\theta(x)}. \tag{1}$$

Initially, we restrict our analysis to the inner radius of the annulus, where x measures the distance along the ring. Let us denote the inner circumference of the ring by C. On quenching from the normal to the superconducting phase, we can define a winding number density $n(x) = \partial_x\theta(x)/2\pi$ along this circumference. In the absence of any external fields the total winding number n around the loop is zero on average, but will have non-zero variance

$$\langle n^2\rangle = \int_0^C \mathrm{d}x \int_0^C \mathrm{d}y\ \langle n(x)\, n(y)\rangle\,, \tag{2}$$

and it is this that we measure, indirectly, through the matching flux generated in the interior of the annulus, which is directly observable. This flux is quantized (as fluxoids) in units of $\Phi_0 = hc/2e$.

Suppose the correlator is described through the single length scale $\bar{\xi}$. For large annuli, for which $C \gg \bar{\xi}$, we can replace equation (2) by

$$\langle n^2\rangle = \frac{C}{2}\int_0^C \mathrm{d}x\ \langle n(x)\, n(0)\rangle \approx \frac{C}{2}\int_0^\infty \mathrm{d}x\ \langle n(x)\, n(0)\rangle\,, \tag{3}$$

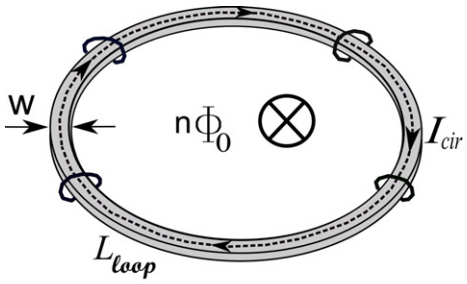

Figure 1. 3D sketch of a superconducting ring of width w with n trapped magnetic flux quanta, in the absence of any external flux. A supercurrent $I_{\rm cir}$ circulates around the ring. The magnetic field lines wrap around the ring section.

if we assume that the two-point correlation function $\langle n(x)\, n(y)\rangle$ is of short range compared to C. Simple dimensional analysis then gives

$$\langle n^2\rangle = aC/\bar{\xi}, \tag{4}$$

the perimeter law assumed in the Kibble–Zurek picture, interpreted as a random walk in phase along the circumference in steps of length $\bar{\xi}$.

To estimate the length scale $\bar{\xi}$ we first repeat the Kibble–Zurek argument of [3, 4], assuming rapid cooling through a continuous transition with transition temperature $T_{\rm c}$. Suppose $\xi(t)$ is the *adiabatic* correlation length for $n(x)$ at time t, diverging at the transition at $t = 0$ as the temperature $T(t)$ changes ($T(0) = T_{\rm c}$). If the system is initially homogeneous and isotropic, the KZ scenario proposes that on approaching the transition the increasing correlation length, originally changing adiabatically, will freeze (the 'impulse' regime) at time $t_< < 0$, when $\dot{\xi}(t_<) \approx c(t_<)$, where $c(t)$ is the relevant causal speed at time t. Equivalently, this can be rephrased in terms of critical slowing down [3, 4].

An alternative approach suggests that, *after* passing through the transition, the system will unfreeze into a new adiabatic regime at a time $t_> > 0$ when $|\dot{\xi}(t_>)| \approx c(t_>)$, and that it is the distance scales here that set the domain size. This gives us the same scaling behaviour and, indeed, it was proposed in the early literature that $t_<$ is as good a time as $t_>$ for estimating domain size [2, 3]. This change of viewpoint—that the relevant dynamics for quantitative behaviour occur after the transition rather than before—is supported by numerical simulations [5].

The correlation length $\bar{\xi}$ that sets the scale for phase change along the ring in equation (4) is estimated to be

$$\bar{\xi} \approx \xi(t_>) = \xi_0 \left(\frac{\tau_{\rm Q}}{\tau_0}\right)^{\sigma}, \tag{5}$$

where ξ_0 and τ_0 are system-dependent and $\tau_{\rm Q}$ is the quench time (the inverse quench rate through the transition). For type-II superconductors $t_> = \sqrt{\tau_0 \tau_{\rm Q}}$ and $\sigma = 1/4$ in the mean-field approximation.

Such scaling behaviour can have a different origin than simple causal unfreezing. Defect formation may be thought of as arising from the growth of unstable long wavelength modes—as the field rolls off the potential 'hill'—rather than through direct causal bounds. This is supported indirectly by the many simulations (e.g. [6–8]) demonstrating the validity of equation (5) based on time-dependent Ginzburg–Landau (TDGL) theory, and we shall give an explicit demonstration later.

This shift of view is crucial when considering laboratory systems. Whereas the early Universe can be taken as homogeneous to a very high degree, the same cannot be said of experiments. One step to limit inhomogeneity is to make the system small. However, this incurs finite size effects. Specifically, the scaling behaviour of equation (5) assumes that $C \gg \bar{\xi}$. However, if we think in terms of growth of mode amplitudes after the quench there are always modes comparable in wavelength to the system size; their growth can still contribute to defect formation.

The KZ length $\bar{\xi}$ can of course be recovered from a picture of expanding mode amplitudes for large systems. If $t_>$ is a guide for the time at which defects form, then it is much smaller than the time taken for the order parameter field(s) to experience the degenerate vacua. If they remain so close to the unstable 'vacuum' that the nonlinearities of the backreaction can be approximately ignored, the effectively linearized field equations give rise to Gaussian field correlation functions. These linearized equations generally lead to KZ scaling behaviour for fast quenches in large systems, both non-relativistic and relativistic [9–11]. More recently, preliminary simulations which further support underlying Gaussian behaviour explicitly for superconductors were performed by us in [12, 13], and this paper builds on this analysis.

For homogeneous small systems with $C < \bar{\xi}$, which are inaccessible to the KZ picture, the Gaussian approximation permits an analytic replacement of equations (4) and (5) which encodes the KZ scale $\bar{\xi}$ despite the smallness of the system. Furthermore, the same Gaussian approximation is applicable to explicit symmetry breaking driven by the application of external fields, for which the KZ scenario again offers little help. This is an interesting problem in its own right and is a serious problem because of the presence of stray fields in the laboratory. Scaling behaviour of the form of equation (5) can only be demonstrated experimentally once external fields have been countered.

This paper is organized as follows. For narrow rings we might hope that the system would behave one-dimensionally; in the next section we reexamine the Gaussian approximation (or rather, two related Gaussian approximations) for both large and small idealized 1D systems. We then show that numerical simulations provide strong support for Gaussian behaviour, both in the power spectrum of field ordering and in the damping of fluxoid generation in small systems. In particular, we explore the way in which the power of field fluctuations is driven into long wavelengths through the growth of unstable modes, in good accord with our Gaussian expectations. We conclude with a discussion of new experimental results for fluxoid production in an external field, and show that it, too, is explicable in terms of Gaussian fluctuations. Good agreement with 3D simulations is observed.

2. Gaussian behaviour for 1D systems

Unsurprisingly, 1D systems are the easiest for which we can make analytic predictions and implement numerical simulations. There are two strongly related variants of the Gaussian approximation that we shall consider; each has its strengths.

2.1. Long superconductors: Gaussian probabilities

The first Gaussian approximation, proposed in [14, 15], is predicated on the perimeter rule, equation (4). We begin by considering a large loop, divided up into N domains, in each of which θ is a constant. We assume that there is no correlation between the values of θ in adjacent domains but that the shortest path in phase (the geodesic rule) will be taken when jumping from one domain to the other. Let $G_N(\Delta\theta)$ be the probability that the change in phase θ is $\Delta\theta$ after the N links that make the loop. The assumed lack of correlation means that the probability of ending with a phase shift of $2\pi m$ (net fluxoid number m) is

$$p_m(N) = \int_{-\pi+2m\pi}^{\pi+2m\pi} \mathrm{d}\Theta\, G_N(\Theta). \tag{6}$$

To bring this into correspondence with the KZ scenario, we should identify the domain size as comparable to $C/\bar{\xi}$, i.e., $C = aN\bar{\xi}$, where $a = O(1)$. With this in mind, we assume that the total phase change $\Delta\theta$ around the loop can be expressed as the sum of a random term Θ and a geodesic-rule correction $\delta\Theta$, necessary to obtain an integer winding number [16]. It is convenient to relax N to be a *continuous* variable. We further assume that Θ has a normal distribution with average $\bar{\Theta} = 0$ and variance σ^2 proportional to N i.e.,

$$G_N(\Theta) = \frac{1}{\sqrt{2\pi\sigma^2(N)}} \exp -\frac{\Theta^2}{2\sigma^2(N)}. \tag{7}$$

The trapping probabilities $p_m = p_{-m}$ are easily found. In particular, since in our experiments we rarely see more than one fluxoid, we are primarily interested in

$$p_0(N) = \mathrm{erf}\left[\frac{\pi}{\sqrt{2\sigma^2(N)}}\right] \tag{8}$$

and

$$\begin{aligned}\bar{p}_1 &= p_1(N) + p_{-1}(N)\\ &= \left[\mathrm{erf}\frac{3\pi}{\sqrt{2\sigma^2(N)}} - \mathrm{erf}\frac{\pi}{\sqrt{2\sigma^2(N)}}\right].\end{aligned} \tag{9}$$

From the large-N behaviour of the p_m it follows that, for large rings, $\sigma^2(N) = 4\pi^2\langle n^2\rangle$. Also, we can identify equation (7) from the central limit distribution by taking $\sigma^2(N) = \frac{\pi^2}{3}N$ for large N. Further details may be found in [16].

2.2. A Gaussian variant: Gaussian distributions

For our second approximation, rather than assume the Gaussian distribution for Θ of equation (7), we assume that the winding number density field $n(x)$ is a Gaussian field [16]. It then follows that the all-important probabilities of finding no fluxoids or one fluxoid are

$$f_0 = \frac{1}{2\pi}\int_{-\pi}^{\pi} \mathrm{d}z\, \exp(-z^2\langle n^2\rangle/2) \tag{10}$$

and

$$\begin{aligned}\bar{f}_1 &= f_1 + f_{-1}\\ &= \frac{1}{\pi}\int_{-\pi}^{\pi} \mathrm{d}z\, \exp(-z^2\langle n^2\rangle/2)\cos z\end{aligned} \tag{11}$$

respectively. We use the notation f_m for the probability of winding number m in this approximation to distinguish it from the p_m of the previous section for Gaussian winding number densities. None of equations (8)–(11) take periodicity into account. In figure 2 we show how the predictions for p_n and f_n are almost indistinguishable, only differing slightly at very small probabilities where periodicity is important.

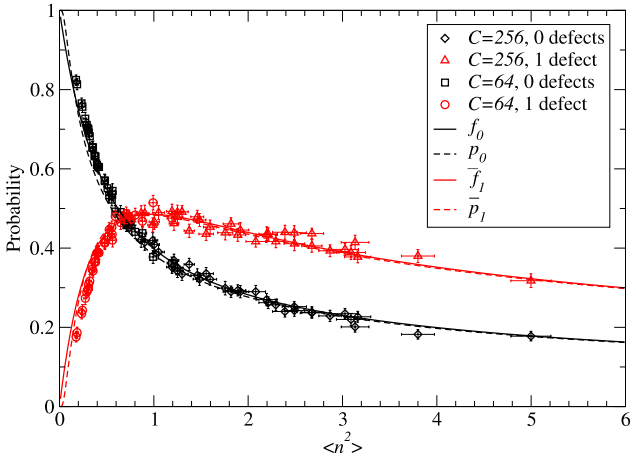

Figure 2. We plot (p_0, f_0) and then $(\bar{p}_1, \bar{f}_1)$ against $\langle n^2\rangle$ for a 1D superconducting ring to show the similarity of the Gaussian approximations. In particular, both $\bar{p}_1$ and $\bar{f}_1$ have maximum values of approximately 0.49. Both are contrasted with the results of the 1D simulation. Because neither approximation takes periodicity into account the likelihood of seeing flux at low levels is overestimated; see figure 4. Otherwise agreement is good within errors.

The Gaussian approximations so far do not give the KZ scaling behaviour of equation (5). To see this we make the further Gaussian approximation that, on decomposing the complex order parameter field as $\phi = (\phi_1 + \mathrm{i}\phi_2)/\sqrt{2}$, ϕ_1 and ϕ_2 are independent Gaussian fields. The correlation function for the winding number density is now determined by the correlation function $G(x)$ for the field components, defined by

$$\langle\phi_a(x)\,\phi_b(y)\rangle = \delta_{ab}G(|x-y|). \tag{12}$$

We next use the fact that, for damped systems, the Gaussian approximation corresponds to a linearization of the TDGL equations. Periodicity is unimportant for large rings and we find (see [17]) that the field correlation function $G(r)$ at the defect formation time for large systems takes the form

$$G(r,t) = \int \frac{\mathrm{d}k}{2\pi}\, \mathrm{e}^{\mathrm{i}kx}P(k,t) \tag{13}$$

in which the power spectrum $P(k, t)$ has a representation in terms of the Schwinger proper-time τ (in the dimensionless units of $\tau_0 = \xi_0 = 1$) as (approximately) [9, 10, 17]

$$P(k,t) \propto \int_0^\infty \mathrm{d}\tau\, \mathrm{e}^{-\tau k^2}\, \mathrm{e}^{-\int_0^\tau \mathrm{d}s\ \epsilon(t-s/2)}, \tag{14}$$

where $\epsilon(t) \equiv T(t)/T_c$ is the reduced temperature. We assume the dependence $\epsilon(t) = -t/\tau_Q$ for a quench linear in time in the vicinity of the phase transition where fluxoid formation takes place. Adopting this $\epsilon(t)$ gives

$$P(k,t) \propto \int_0^\infty \mathrm{d}\tau\, \mathrm{e}^{-\tau k^2}\, \mathrm{e}^{t\tau/\tau_Q}\, \mathrm{e}^{-\tau^2/4\tau_Q}; \tag{15}$$

$P(k) \propto k^{-2}$ for large k^2. In the dimensionless units above, the time for the formation of fluxoids is $O(t_>) = O(\sqrt{\tau_Q})$. When $D \geq 2$ the integral is dominated by the ultraviolet for slow quenches, which needs to be cut off at distance scale ξ_0.

It remains to convert the Gaussian behaviour of the fields into the Gaussian behaviour of the winding number. We observe that

$$n(x) \equiv \frac{1}{|\phi(x)^2|}\bar{n}(x) = \frac{1}{|\phi(x)^2|}\left(\phi_1\partial_x\phi_2 - \phi_2\partial_x\phi_1\right). \tag{16}$$

A simple approximation, sufficient for our purposes, is to take [18]

$$\begin{aligned}\langle n(x)n(0)\rangle &\approx \frac{\langle \bar{n}(x)\,\bar{n}(0)\rangle}{\langle|\phi^2|\rangle^2} \\ &= \frac{2}{(2\pi)^2}\left[f'(x)^2 - f''(x)f(x)\right],\end{aligned} \tag{17}$$

where $f(x) = G(x)/G(0)$. Provided quenches are fast enough that we can ignore the ultraviolet effects, it follows from equation (15) that f takes the Gaussian form

$$f(r) \approx \mathrm{e}^{-r^2/2\xi_r^2} \tag{18}$$

for small $r = |x|$. Note that this is evaluated at the KZ time $t_> \approx \tau_Q^{1/2}$, hence we have $\xi_r \approx \bar{\xi}$, the KZ separation length [9, 10]. This is appropriate for a damped system at short distance.

This creation of winding number can be thought of as due to the unstable long wavelength modes of the field growing as fast as possible, with no backreaction in the short time necessary. It follows that, on restoring dimensional units,

$$\langle n^2\rangle \approx a\frac{C}{\xi_0}\left(\frac{\tau_Q}{\tau_0}\right)^{-\sigma}. \tag{19}$$

All the above continues to ignore periodicity. The advantage of choosing Gaussian *fields* is that they permit the imposition of periodic boundary conditions in a way that the Gaussian distributions described above do not.

2.3. Small annuli: Gaussian approximation

We would expect that small systems, whether superconductors or not, would show proportionately less defect production per unit length than larger systems because of end effects or periodicity. Let us consider small annuli for which $C/\bar{\xi} \ll 1$.

The periodicity of $f(x)$ in x (mod C) is now important. The effect of periodicity is to discretize k in equation (15). To implement this in the approximation of equation (18), we need to replace $f(x)$ by its periodic generalization, the Jacobi ϑ function [12]

$$f(x)_{\mathrm{per}} = \frac{\vartheta_3(\pi x/C|2\pi\mathrm{i}\xi_r^2/C^2)}{\vartheta_3(0|2\pi\mathrm{i}\xi_r^2/C^2)} \tag{20}$$

$$\approx 1 - 4\sin^2(\pi x/C)\,\mathrm{e}^{-2\pi^2\xi_r^2/C^2}, \tag{21}$$

whence, from equation (2),

$$\langle n^2\rangle = \mathcal{O}(\mathrm{e}^{-4\pi^2\xi_r^2/C^2}). \tag{22}$$

Thus, rather than the power falloff for large loops we have exponential damping

$$\ln\langle n^2\rangle \approx -4\pi^2\xi_r^2/C^2 + \mathrm{const.} \tag{23}$$

Since it is small, $\langle n^2\rangle \approx f_1$, the probability of finding a single winding number along the annulus. In principle $\xi_r \propto \tau_Q^\sigma$, but some caution is necessary in that the approximation of equation (17) is too simple, which makes the single term in equation (23) only approximate, although it preserves the correct features [18]. In [12] we showed that exponential damping does take place. However, we can go further in that, if we combine equation (19) for $\sigma = 1/4$ with equation (23), then in units $\xi_0 = \tau_0 = 1$

$$\langle n^2\rangle = F(\tau_Q/C^4) \tag{24}$$

for some function F interpolating between power behaviour and exponential damping that covers all sized annuli and quench rates.

2.4. Numerical simulations

We simulate our 1D superconductor with the U(1) scalar field theory of the complex order parameter ϕ, given previously, on a ring of circumference C with periodic boundary conditions. To mimic a temperature quench through its critical point at time $t = 0$ we take an explicitly time-dependent potential

$$V(|\phi|^2) = \epsilon(t)|\phi|^2 + \tfrac{1}{2}b|\phi|^4. \tag{25}$$

Rather than just take ϵ linear in t, as we did in equation (15), we now adopt the more realistic behaviour

$$\epsilon(t) = \begin{cases} 1, & t < -\tau_Q, \\ -t/\tau_Q, & -\tau_Q < t < \tau_Q, \\ -1, & t > \tau_Q, \end{cases} \tag{26}$$

to model a slow quench. We start at $t = -2\tau_Q$ and continue until $t = 4\tau_Q$, by which time the defects have frozen out. This system is modelled by a damped second-order Langevin equation with zero mean Gaussian noise. Our linearized Gaussian approximations are independent of b in the first instance; we have performed our simulations for varying b without any noticeably different results. In evolving the equations a stochastic leapfrog method is used [19]. Further details may be found in [12].

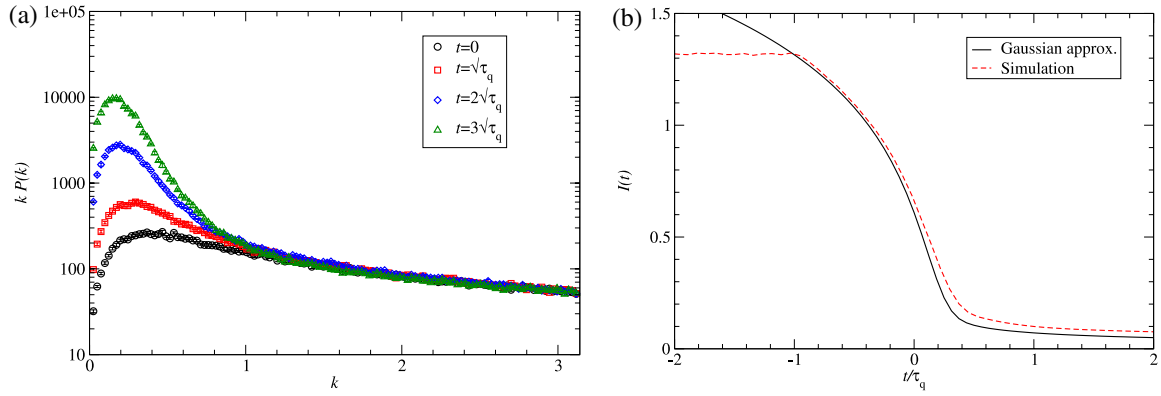

Figure 3. (a) We plot $kP(k)$ against k for a variety of $t > 0$, in multiples of the KZ time $t_> = \sqrt{\tau_Q}$ for $\tau_Q = 32$ on a lattice of size $C = 256$. The characteristic wavelength increases with increasing time as the field orders itself. (b) We plot the first moment of $P(k)$ from the simulation and compare it to its value from (15). An identifiable scaling length is only established for $t \gtrsim 3t_>$. This is reasonable from the KZ viewpoint since $t_>$ is the *minimum* time at which the system could unfreeze.

Our first application of this simple simulation is to test the validity of our Gaussian approximations discussed earlier. In figure 2 we show the observed frequencies for trapping a given number of fluxoids as a function of $\langle n^2 \rangle$. This is compared with the Gaussian predictions (p_0, f_0) and $(\bar{p}_1, \bar{f}_1)$. The agreement is surprisingly good. In particular, the Gaussian upper bound on finding a single fluxoid at about 0.49 that follows from equations (11) and (9) is saturated in the simulation (within errors). This supports the Gaussian approximation in its simplest guise.

We can say more. The analysis that led to equations (14) and (15) for the power spectrum of the fluctuations is dimension independent and only relies on the Gaussian nature of the fields. As the fields become ordered the power is driven into longer wavelengths. This can be seen most simply by looking at moments of $P(k)$, for which we expect a peak at $\bar{k} \approx \bar{\xi}^{-1}$. As an example, in figure 3 we take the first moment

$$I(t) = \frac{\int_0^{2\pi} \mathrm{d}k\, kP(k)}{\int_0^{2\pi} \mathrm{d}k\, P(k)} \tag{27}$$

for a given τ_Q, since it is less susceptible to the UV cutoff $k = 2\pi$ (corresponding to a length cutoff at $O(\xi_0)$ in our dimensionless units). In figure 3(a) we plot $kP(k)$ from the numerical simulation for $t > 0$ in multiples of $\sqrt{\tau_Q}$. As we expect, the power gets pushed into longer and longer wavelengths. The scale over which that happens becomes clearer if we plot the moment $I(t)$. In figure 3(b) we compare $I(t)$ measured in the simulation to the analytic behaviour derived from equation (15). $I(t)$ is seen to stabilize at a value proportional to $\bar{\xi}^{-1}$ by the time defects form. The Gaussian approximation drives the power to longer wavelengths than the simulation but, as we know from elsewhere [17], the scaling behaviour of the dominant wavelength (corresponding to $\bar{\xi}^{-1}$) remains the same.

3. Annular superconductors in three dimensions

Even thin annuli are not one-dimensional and we should take the annulus width into account. Moreover, even a superconductor that is effectively a 2D film cannot be treated entirely as two-dimensional since the three-dimensional nature of the flux lines cannot be ignored. In fact, the KZ analysis is potentially incomplete, in that the possibility exists of long wavelength modes of the electromagnetic field freezing in as the transition is implemented. However, we have seen previously (in [13]) that this secondary mechanism, the Hindmarsh–Rajantie (HR) mechanism [20, 21], does not seem to be important for our small systems and we shall not pursue it further.

3.1. The 2D Gaussian approximation

For the moment we restrict ourselves to the complex field $\phi_a(\mathbf{x})$, extended now to the x_1–x_2 plane, assumed Gaussian, as before. As it stands it is too difficult to get analytic results for arbitrary annuli so, as a first step, we consider a 2D superconducting film of infinite extent and we look for the behaviour of the winding number along a circular closed loop in the film of circumference C, that encloses a surface S.

If $\rho_3(\mathbf{x})$ is the topological density in the plane [22, 23], for given field configurations $\phi_a(\mathbf{x})$ the phase change θ_C along the path can be expressed as the surface integral

$$\theta_C = 2\pi \int_{\mathbf{x}\in S} \mathrm{d}^2x\ \rho_3(\mathbf{x}) = -2\pi \int_{\mathbf{x}\notin S} \mathrm{d}^2x\ \rho_3(\mathbf{x}) \tag{28}$$

from charge conservation. It then follows that, for Gaussian fields, $\langle n^2 \rangle$ satisfies

$$\langle n^2 \rangle = -\int_{\mathbf{x}\notin S} \mathrm{d}^2x \int_{\mathbf{y}\in S} \mathrm{d}^2y\ \langle \rho_3(\mathbf{x})\rho_3(\mathbf{y}) \rangle, \tag{29}$$

where $\mathbf{x}$ and $\mathbf{y}$ are in the plane of S. Using the results of [22, 23] it is not difficult to express the density correlation in terms of the field correlation $f(r)$ $(r = |x|)$,

$$\langle \rho_3(\mathbf{x})\rho_3(\mathbf{0}) \rangle = \frac{1}{4\pi^2 r} \frac{\partial}{\partial r} \left(\frac{f'(r)^2}{1 - f(r)^2} \right). \tag{30}$$

It follows from equation (18) that the density correlation has a range $O(\xi_r)$. With $\mathbf{x}$ outside S, and $\mathbf{y}$ inside S, all the

contribution to $\langle n^2 \rangle$ comes from the vicinity of the boundary of S, rather than the whole area. For large rings this means that if we removed all material except for a strip of width $O(\bar{\xi})$ from the neighbourhood of the contour C we would still have the same result. As before, this gives the perimeter rule

$$\langle n^2 \rangle \approx a \frac{C}{\xi_r}. \tag{31}$$

That is, we have the anticipated random walk in phase along the contour, from which we recover the canonical scaling of equation (5) on identifying ξ_r.

For small annuli the situation is less clear. While the behaviour of equation (29) suggests that the winding number along a small closed path in a 2D superconducting film is proportional to the area of the ring (and hence doubles the KZ exponent), it is not clear that this behaviour would be preserved if the interior of the closed path were removed to make a broad annulus. A test of this is to preserve the perimeter of the annulus but to take different aspect ratios (i.e. different areas). A perimeter law would leave probabilities unchanged, but an area law would lead to differences. The relevance of this is that in an earlier experiment [24], results suggested a doubling of the KZ exponents—albeit with large errors.

3.2. Simulations

To test the approximations outlined in the previous sections we simulated the superconducting ring in a 3D box [13]. Although the superconductor is thereby taken to be a thin planar film, the three-dimensional simulation allows for nontrivial correlations of the magnetic field. Periodic boundary conditions are used. The quench protocol is the same as for the 1D simulations, meaning that $\epsilon(t)$ is of the form given in equation (26).

We first sought to see whether the exponential falloff in trapping probability predicted above by 1D simulations was the same for the more realistic theory of 2D rings in three dimensions. In figure 4, we show the crossover from KZ behaviour to exponential damping as a function of the combination τ_Q/C^4, for both the 1D and 3D systems discussed above. While there is complete agreement for large annuli, the exponential damping for small annuli is dimension-dependent. This is perhaps because of the differences between the 1D expression equation (17) and the 2D equivalent (30), on substituting equation (21) for $f(r)$, even though the annulus is not particularly wide [25]. As we would have anticipated, this difference is insensitive to self-coupling strength, as we have checked (but not displayed).

4. External fields

All the analysis above assumed no external fields. Experimentally, this is unrealistic. Moreover, driven symmetry breaking through the application of external bias is an interesting question in its own right. The KZ scenario cannot address this, but we shall find that we can obtain results in the Gaussian approximation that can be analysed in simulations.

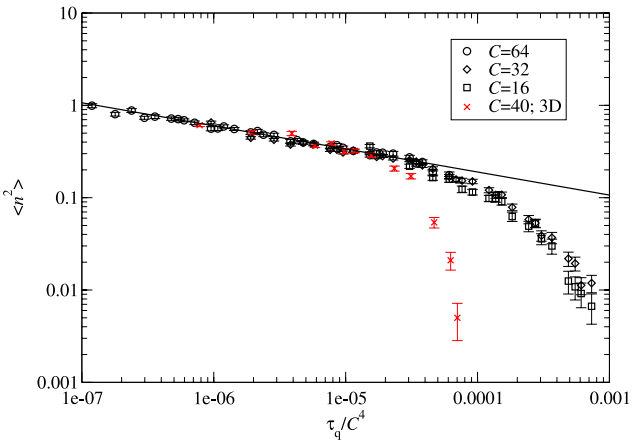

Figure 4. Results of simulations for annuli with inner circumference C in 1D and 3D, as a function of τ_Q/C^4. In both a change in behaviour from KZ scaling to exponential suppression occurs. We see that there is complete agreement for large annuli (fast quenches) and different exponential damping for small annuli (slow quenches).

Experimentally, we compensate for unknown stray fields by applying an external bias field to cancel them. We know this has happened when the likelihood of seeing spontaneous flux is at a minimum. To do this successfully we need to know the likelihood of fluxoid production in the presence of external fields. It is difficult to extend the previous analysis with periodic boundary conditions to include external fields and we adopt a simpler straightforward variant of the Gaussian approximation.

4.1. Fluxoid production in an external field: 1D approximation

Let us now apply a magnetic flux Φ_f to the loop; this breaks the $\theta \to -\theta$ symmetry. The effect of Φ_f is to produce a non-zero average winding number $\langle n \rangle = \bar{n}(\Phi_f) = \Phi_f/\Phi_0$ after the transition, where $\Phi_0 = hc/2e$.

Because of the limitations of one dimension, the electromagnetic field can only be introduced classically. The natural extension of our Gaussian probability model [16], $G_N(\Theta)$ in equation (7), for a superconducting loop linked to a magnetic flux Φ_f is that the phase distribution will still be normal with the same variance $\sigma^2(N)$, but with non-zero average $\bar{\Theta}(\Phi_f) = 2\pi\bar{n}(\Phi_f) = 2\pi\Phi_f/\Phi_0 = 2\pi\phi_f$,

$$G_N(\Theta, \phi_f) = \frac{1}{\sqrt{2\pi\sigma^2(N)}} \exp - \frac{(\Theta - 2\pi\phi_f)^2}{2\sigma^2(N)}. \tag{32}$$

With such a distribution, the probability p_m of ending up with a given winding number m is given by

$$p_m(\phi_f) = \int_{-\pi+2m\pi}^{\pi+2m\pi} \mathrm{d}\theta \; G(\theta; \phi_f). \tag{33}$$

That is

$$p_{\pm m}(N, \phi_f) = \frac{1}{2}\left[\mathrm{erf} \frac{(\pm 2m - 2\phi_f + 1)\pi}{\sqrt{2\sigma^2(N)}} - \mathrm{erf} \frac{(\pm 2m - 2\phi_f - 1)\pi}{\sqrt{2\sigma^2(N)}} \right], \tag{34}$$

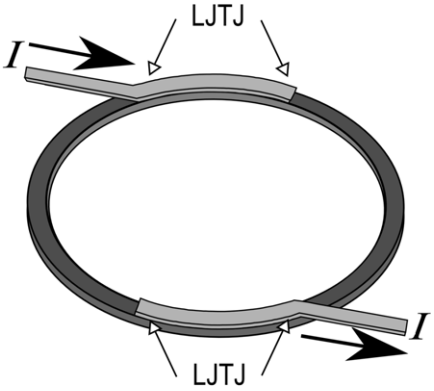

Figure 5. The magnetic field associated with the trapped fluxoids can be detected by one or more long Josephson tunnel junctions, where the base electrode (dark grey) is formed by the ring itself. The top electrodes of the two planar Josephson tunnel junctions are in light grey.

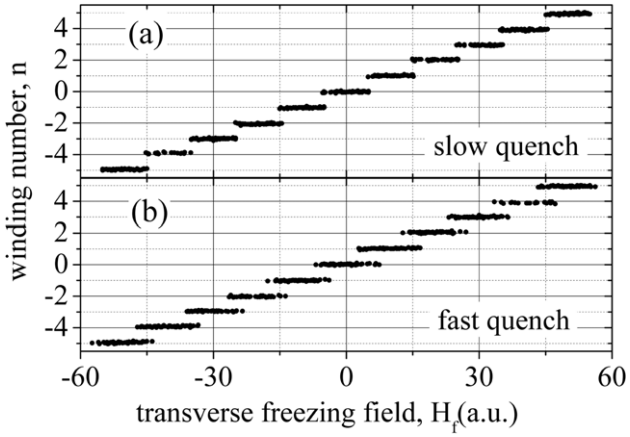

Figure 6. The winding number, n, versus the magnetic transverse field, H_f, with which the loop was field-cooled through its superconducting transition temperature, $T_\mathrm{c} \approx 9.1$ K. (a) Slow quench: the temperature rate change, $\mathrm{d}T/\mathrm{d}t$, during the cooling through the critical temperature was -0.5 K ms^{-1}; (b) fast quench: $\mathrm{d}T/\mathrm{d}t \sim -50$ K ms^{-1}. The horizontal and vertical offsets are arbitrary. Note that H_f was switched off during the readout.

which, in the presence of a possible stray or residual flux ϕ_r, we reparametrize as

$$p_m(\phi_\mathrm{f}) = \frac{1}{2}\left[\mathrm{erf}\,\frac{\phi_\mathrm{f} - \phi_\mathrm{r} - m + 0.5}{s_\mathrm{d}} - \mathrm{erf}\,\frac{\phi_\mathrm{f} - \phi_\mathrm{r} - m - 0.5}{s_\mathrm{d}}\right], \qquad (35)$$

where the dependence on quench time and geometry is parameterized by $s_\mathrm{d} \equiv \sqrt{2\sigma^2(N)/2\pi}$. Now, $p_{+m}(\phi_\mathrm{f}) \neq p_{-m}(\phi_\mathrm{f})$. Essentially, what really matters is the difference $m - \phi_\mathrm{f}$; for example, $p_m(1) = p_{m-1}(0)$. This calculation unfortunately does not allow us to determine the dependence of s on τ_Q. Nevertheless, we can fit data for different applied magnetic fields at fixed τ_Q to equation (35) with only s_d and ϕ_r as free parameters to yield f_0.

We have seen that the Gaussian probability is a good approximation for large rings and, as before, we extrapolate to small rings, using equation (34) as it stands.

5. Experiments in an external field

For a thin-film loop, of width w much larger than its thickness but smaller than the ring radius, the intensity of the radial magnetic field H_ρ at the film surface is (see figure 1)

$$H_\rho = \frac{I_\mathrm{cir}}{2w} = \frac{n\Phi_0 - \Phi_e}{2wL_\mathrm{loop}}. \qquad (36)$$

Equation (36) indicates that a superconducting loop acts as a flux-to-field transformer; if a magnetic sensor is placed above (or below) part of the loop, it will thus detect the local radial field H_ρ and hence the magnetic flux Φ_e linked to the loop and the winding number, n. In this context, the most natural magnetic sensors are planar Josephson tunnel junctions. More specifically, the critical current of a long Josephson tunnel junction (LJTJ)—for which the loop itself constitutes one of the superconducting electrodes—is able to resolve flux changes well below the flux quantum [26]. Figure 5 shows a superconducting ring acting as the base electrode for two LJTJs. Let us stress that the critical current of an LJTJ is sensitive to the surface field, H_ρ, whereas the superconducting loop is only sensitive to the perpendicular field, $H_\perp$.

Figures 6(a) and (b) show the quantum levels observed when the system is cooled through a controlled normal–superconducting (NS) transition in the presence of a transverse magnetic field, H_f, which is incremented by steps corresponding to $\sim 0.02\,\Phi_0$ jumps in the freezing flux, $\Phi_\mathrm{f} = \mu_0 H_\mathrm{f} A_\mathrm{loop}$, where A_loop is the loop area. Once H_f is removed, each trapped flux quantum results in a small change in H_ρ which, in turn, produces a detectable change in the junction zero-field critical current, I_c. The two panels of figure 6 refer to the same sample quenched in the same field range, but with different cooling rates, $\mathrm{d}T/\mathrm{d}t$. In the first panel the cooling rate is about -500 K s^{-1}, while it is a hundred times larger for the second panel, where a marked overlap of the quantum states is visible. In deriving figures 6(a) and (b), we assumed that the (unknown) residual magnetic field of our setup was small enough to be trapped in the loop as less than one fluxoid. Nevertheless, the presence of any larger (static) magnetic field would simply result in a horizontal shift of the field axis or, correspondingly, a vertical shift of the winding number, n. In other words, we are able to measure the changes in the loop quantum state, but not its absolute value. Luckily, as discussed in section 4.1, the transition from the nth to the $(n+1)$th state is virtually independent of n.

5.1. Equipment used

Our setup consisted of a cryoprobe inserted vertically in a commercial LHe dewar. The cryoprobe was magnetically shielded by means of two concentric Pb cans and a vacuum tight cryoperm can surrounding them and immersed in the LHe bath ($T \simeq 4.2$ K). In addition, the measurements were carried out in an RF-shielded environment. We used high quality all-niobium LJTJs fabricated on 4.2×3 mm^2 silicon

substrates using the trilayer technique; the Josephson junction is realized as a window opened in a SiO_2 insulator layer. The samples' parameters can be found in [26].

The chip was mounted on a massive Cu block. Inside the outer can He exchange gas with a pressure of about 20 mbar provided the thermal link between the Cu block and the LHe bath. The chip was heated above the loop critical temperature, $T_c \approx 9.1$ K, by a laser pulse transmitted along an optical fibre to the back side of the chip. The single crystalline Si chip absorbed a large fraction of the incident green light, and its very high thermal conductance minimized thermal gradients. After the laser pulse, excess heat diffuses away from the chip through the thermal contact with the Cu block and the He gas inside the can; the chip temperature then relaxes down to the bath temperature.

During the transition from the normal to the superconducting states, a calibrated magnetic field $H_\perp$ was applied perpendicular to the loop plane by means of a superconducting cylindrical coil aligned with the loop axis, while the LJTJ was electrically isolated; in fact, both the junction voltage and current leads were open during the whole thermal cycle. At the end of each cycle, the transverse field was removed and—as previously explained—the possible fluxoids were counted by a measurement of the LJTJ's zero-field critical currents. This method works well as long as the probability f_2 of trapping two fluxoids is small. Hundreds of thermal cycles were carried out for each value of the trapping field, $H_\perp$; the field value was increased in steps of about $0.1 - 0.2\Phi_0$ until a total flux variation, $\Delta\Phi_f$, well above one flux quantum was achieved. In order to run batches of several thousand thermal cycles with given constant parameters, automation of the thermal cycles was implemented by means of a switching unit controlled by a GPIB interface; this also allowed for more robust statistics to be achieved. At the end of each thermal quench, the zero-field junction current–voltage characteristic was automatically digitally acquired and stored.

The temperature dependence of the LJTJ's gap voltage was used as an on-chip fast thermometer, to monitor the chip temperature during the thermal cycle. The quench time, τ_Q, was inferred from a well known fitting procedure [14]. Figure 7 shows that the quench time τ_Q is proportional to the laser pulse duration Δt, with the proportionality constant almost independent of the sample (and of its mounting procedure). Indeed, this method for reading the loop winding number using an LJTJ was adopted in a previous work [24], but it became reliable and efficient only when the δ-biased [27] junction was replaced by an in-line one [26, 28, 29], as shown in figure 5.

5.2. Fluxoid readout

The discrete variation ΔI_c of the zero-field critical current associated with each flux quantum trapped in the loop is [26]

$$\Delta I_c = g\frac{\Phi_0}{L_{loop}}, \tag{37}$$

where g is a dimensionless parameter of the order of unity that depends on some geometrical details [26]. With a loop

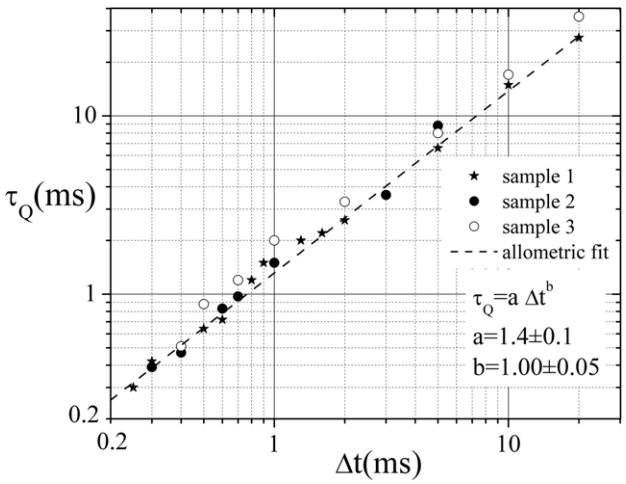

Figure 7. The quenching time, τ_Q, versus the duration, Δt, of the laser pulse for three samples. The dashed line shows the best allometric fit.

inductance $L_{loop} \approx 100$ pH, equation (37) provides I_c jumps of the order of several microamperes in a flux range of hundreds of flux quanta [30]. The discreteness of the critical current values is wider when the loop has a top junction electrode that is narrower and thicker than the bottom one, resulting in a larger gain factor g [31]. The validity of equation (37) is supported by measurements on a number of devices based on narrow loops with annular and rectangular geometries.

5.3. Common mode

In the common mode configuration, shown in figure 5, the two LJTJs share the same doubly connected base electrode and are series biased. Any circulating current, I_{cir}, modulates the zero-field critical currents, I_{c1} and I_{c2}, of the two LJTJs with opposite sign. As a result their difference, $\delta I_c = I_{c2} - I_{c1}$, changes twice as fast as the winding number, n. The rms current noise on δI_c is only $\sqrt{2}$ times larger than that on a single critical current, meaning that in the common mode configuration the signal-to-noise ratio is enhanced by a factor of $\sqrt{2}$. Furthermore, by reading the two critical currents simultaneously and looking at their correlation, it is possible to exclude unwanted events from the statistical analysis. These are related to the trapping of Abrikosov vortices found at pinning centres of the superconducting electrodes. A further reduction of the signal-to-noise ratio by a factor of $\sqrt{2}$ is achieved by taking the combination $I^+_{c2} - I^-_{c2} - I^+_{c1} + I^-_{c1}$, where $I^+_{c1,2}$ and $I^-_{c1,2}$ are the absolute values of, respectively, the positive and negative critical currents of the two LJTJs.

5.4. Measuring the trapping frequency

Figure 8(a) shows the zero-field critical currents, I_{c1} and I_{c2}, of a two-junction annular sample during a statistical batch in which each value of the cooling field, $H_\perp$, was maintained for about a thousand thermal cycles. Since each cycle lasts slightly less than 4 s, the set of 15 000 cycles required about 12 h. The reduction of the critical currents observed during the

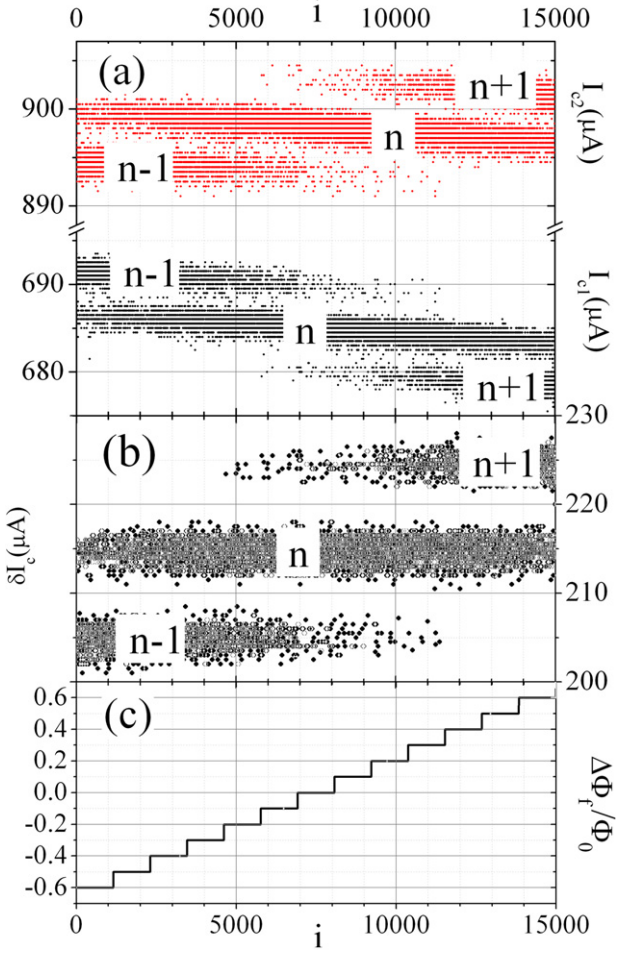

Figure 8. (a) Zero-field critical currents I_{c1} (dark points) and I_{c2} (light points) as a function of the cycle number i. (b) The same for $\delta I_c = I_{c2} - I_{c1}$. (c) Relative variation of the freezing flux, Φ_f. All plots have an arbitrary vertical offset.

measurements corresponds to a small decrease (drift) of the bath temperature. Next, figure 8(b) plots the difference $\delta I_c = I_{c2} - I_{c1}$; we observe that the current jumps have doubled, the signal-to-noise is lower and, in addition, the effect of temperature drift has been counterbalanced. As figure 8(c) indicates, the cycle number i shows the step-like dependence of the freezing flux, Φ_f, as time goes by. Let us call Φ_r the residual magnetic flux; then, to reproduce the zero-flux condition during the quench, a freezing flux $\Phi_f = -\Phi_r$ needs to be applied. Since Φ_r is, in general, unknown, it is necessary to span Φ_f over a range at least as large as one flux quantum.

From the statistical analysis of data thus obtained it is possible to determine the frequency distributions, f_m. Two examples of the frequency dependence on the external field are given in figures 9(a) and (b); we additionally plot 3D simulations for comparable zero-field fluxoid production frequencies in figure 10. The data are very nicely fitted by the Gaussian form of equation (35).

Unfortunately, we do not have enough experimental data to show how $\bar{p}_1$ varies with τ_Q, except that it is in the exponentially suppressed regime.

6. Conclusions

In this paper we have explored the ways in which spontaneous fluxoid production in annular superconductors can cast light on the Kibble–Zurek (KZ) mechanism in systems that are far from equilibrium.

The simple picture is complicated by two effects: small size and symmetry-breaking external fields. The KZ scenario is unable to address either of these. However, we know that the basic scaling result, equation (5), also provides a good test of the Gaussian behaviour of the order parameter field at the time of fluxoid production, in a way that correctly encodes the KZ scales. We have extended the Gaussian approximation to those areas that the KZ scenario cannot reach.

As it stands, the Gaussian approximation is only simply analytic for an idealized 1D annulus, in which we can include an external magnetic field classically. In fact, we have adopted two variants of Gaussianity that differ very slightly: one is more convenient for addressing periodicity; the other for including external fields. We have performed more

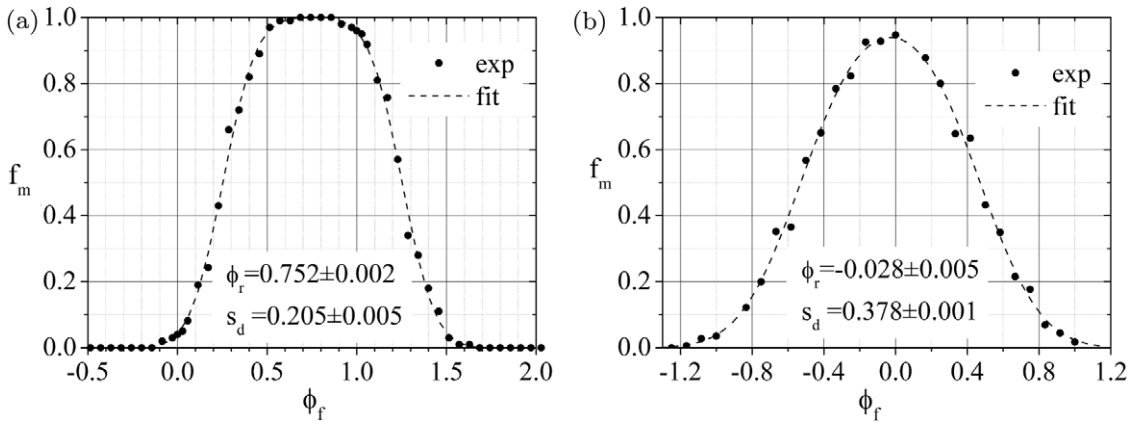

Figure 9. Experimental probability $\bar{p}_1$ of observing one defect as a function of normalized external magnetic flux ϕ_f. The curves are fits of the form given in equation (35).

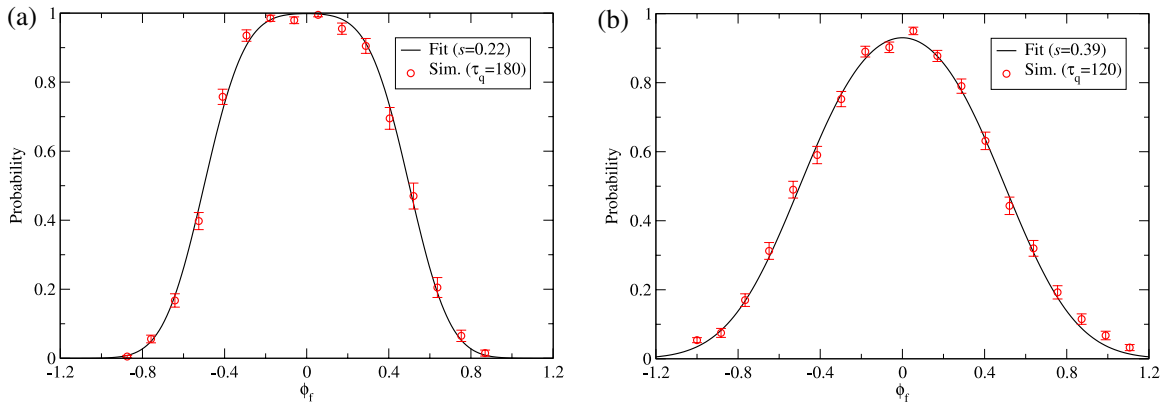

Figure 10. As figure 9 but for 3D simulations with a non-zero external field [13]. The peak probabilities are comparable. The experimental measurements, the simulations and the Gaussian approximation all agree.

simulations based on TDGL theory, both for the idealized 1D annulus and for a more realistic annulus with finite width embedded in 3D space. Where comparable, we find no important difference between the 1D and 3D simulations.

For large rings we reproduce the canonical KZ scaling. However, the likelihood of seeing fluxoids for small ring size or slow quenches is exponentially damped in a dimensionally dependent way.

In the presence of the explicit symmetry breaking of external fields we find strong agreement between the 3D simulations and the 1D results of the Gaussian approximation. Indeed, experimental results for Nb annuli agree totally with both. The implications for the KZ scenario are strong. Rather than think in terms of causal horizons as the constraints on growth of correlations, we see field ordering in terms of the fastest possible growth of unstable long wavelength modes, while encoding KZ scales.

We finish with an important issue that requires further study. This is the empirical observation of scaling behaviour in this, and other, systems for which the observed exponents initially take double the canonical KZ values, as seemed to be the case in our earlier experiment on superconducting annuli [24]. Further, a recent experiment on defect production in linear ionic crystals again shows twice the expected exponent [32]. We believe there are different reasons for these. In [24] we provided a possible Gaussian explanation for superconductors in terms of small size effects, which was applied by the authors of [32]. Preliminary analyses here suggest something more complicated. The conditions imposed in [24] for doubling in 1D systems are not satisfied for superconducting loops. Unless there is an effect due to annulus width (which Gaussianity suggests for wide annuli but which we have been unable to reproduce in simulations), our 'doubling' of [24]—with its large errors in comparison to those of [14, 33]—is most likely the shoulder in figure 4 as the exponential damping takes hold. Indeed, recent experiments involving Josephson vortices in Bose–Einstein condensates show similar exponential behaviour [34].

The situation is different for short linear systems with open boundary conditions for double-well Z_2—rather than $U(1)$—symmetry breaking, where we do seem to see doubling of the exponent in simulations (not presented here). This is more relevant to linear ionic crystals, giving a possible way to understand empirical exponent doubling seen there [32].

The doubling of KZ scaling exponents for fluxon production in annular Josephson tunnel junctions (presented in [33, 14]) is the most complicated of all. On the one hand, it may be due to the fabrication of the junction, a proximity effect arising from the deposition of non-superconducting metal on the oxide interface. There is possibly another cause, the presence of pinning centres for vortices. Considering a short Josephson tunnel junction as an idealization of a narrow annular junction with a strong pinning centre, an analogous doubling effect to that seen in Z_2 symmetry breaking may take place [35]. This is under study.

Acknowledgments

The authors wish to thank Arttu Rajantie for helpful discussions. RR thanks the Helsinki Institute of Physics for hospitality, where some of this work was performed. The simulations were carried out using the resources of the Imperial College High Performance Computing Service.

References

[1] Kibble T W B 1976 *J. Phys.* A **9** 1387
[2] Kibble T W B 1980 *Phys. Rep.* **67** 183
[3] Zurek W H 1985 *Nature* **317** 505
[4] Zurek W H 1996 *Phys. Rep.* **276** 177
[5] Antunes N D, Gandra P and Rivers R J 2006 *Phys. Rev.* D **73** 125003
[6] Laguna P and Zurek W H 1997 *Phys. Rev. Lett.* **78** 2519
Yates A and Zurek W H 1998 *Phys. Rev. Lett.* **80** 5477
[7] Antunes N D, Bettencourt L M A and Zurek W H 1999 *Phys. Rev. Lett.* **82** 2824
[8] Bettencourt L M A, Antunes N D and Zurek W H 2000 *Phys. Rev.* D **62** 065005
[9] Karra G and Rivers R J 1997 *Phys. Lett.* B **414** 28
[10] Karra G and Rivers R J 1998 *Phys. Rev. Lett.* **81** 3707
[11] Moro E and Lythe G 1999 *Phys. Rev.* E **59** R1303
[12] Weir D J and Rivers R J 2011 *J. Phys.: Conf. Ser.* **286** 012056

[13] Weir D J, Monaco R and Rivers R J 2013 *J. Low Temp. Phys.* **171** 788–96
[14] Monaco R, Mygind J, Aaroe M, Rivers R J and Koshelets V P 2006 *Phys. Rev.* B **74** 144513
[15] Rivers R J, Monaco R, Mygind J, Aaroe M and Koshelets V P 2008 *Phil. Trans. R. Soc.* A **366** 2871
[16] Monaco R, Aaroe M, Mygind J, Rivers R J and Koshelets V P 2008 *Phys. Rev.* B **77** 054509
[17] Rivers R J 2001 *J. Low Temp. Phys.* **124** 41
[18] Swarup A 2006 Investigations into condensed matter analogues of phase transitions in the early universe and other low-dimensional phase transitions *Imperial College Thesis*
[19] Borrill J and Gleiser M 1997 *Nucl. Phys.* B **483** 416
[20] Hindmarsh M and Rajantie A 2000 *Phys. Rev. Lett.* **85** 4660
[21] Rajantie A 2001 *J. Low Temp. Phys.* **124** 5
[22] Halperin B I 1981 *Physics of Defects* (*Proceedings of Les Houches, Session XXXV 1980 NATO ASI*) ed Balian, Kléman and Poirier (Amsterdam: North-Holland) p 816 (at press)
[23] Liu F and Mazenko G F 1992 *Phys. Rev.* B **46** 5963
[24] Monaco R, Mygind J, Rivers R J and Koshelets V P 2009 *Phys. Rev.* B **80** 180501
Kirtley J R and Tafuri F 2009 *Physics* **2** 92
[25] Rivers R J, Kavoussanaki E and Karra G 2000 *Condens. Matter Phys.* **3** 133
[26] Monaco R, Mygind J and Koshelets V P 2012 *Phys. Rev.* B **85** 094514
[27] Monaco R, Mygind J, Koshelets V P and Dmitriev P 2010 *Phys. Rev.* B **81** 054506
[28] Ferrel R A and Prange R E 1963 *Phys. Rev. Lett.* **10** 479
[29] Owen C S and Scalapino D J 1967 *Phys. Rev.* **164** 538
[30] Monaco R 2012 *Supercond. Sci. Technol.* **25** 115011
[31] Monaco R, Koshelets V P, Mukhortova A and Mygind J 2013 *Supercond. Sci. Technol.* **26** 055021
[32] Pyka K *et al* 2012 arXiv:1211.7005
[33] Monaco R, Mygind J, Aaroe M, Rivers R J and Koshelets V P 2006 *Phys. Rev. Lett.* **96** 180604
[34] Su S-W, Gou S-C, Bradley A, Fialko O and Brand J 2013 arXiv:1302.3304
[35] Gordeeva A V and Pankratov A L 2010 *Phys. Rev.* B **81** 212504